

Article

Simulation of Ground Stress Field and Advanced Prediction of Gas Outburst Risks in the Non-Mining Area of Xinjing Mine, China

Jilin Wang ^{1,2,*} , Ming Li ^{1,2}, Shaochun Xu ³, Zhenghui Qu ^{1,2} and Bo Jiang ^{1,2}

¹ Key Laboratory of CBM Resources and Reservoir Formation Process, Ministry of Education (China University of Mining & Technology), Xuzhou 221116, China; cumtmingli@163.com (M.L.); quzhenghui@cumt.edu.cn (Z.Q.); jiangbo@cumt.edu.cn (B.J.)

² School of Resources and Earth Science, China University of Mining and Technology, Xuzhou 221116, China

³ Department of Computer Science, Algoma University, Sault Ste Marie, ON P6A2G4, Canada; Simon.Xu@algonau.ca

* Correspondence: wang4437@cumt.edu.cn; Tel.: +86-516-8359-1000

Received: 21 March 2018; Accepted: 3 May 2018; Published: 17 May 2018



Abstract: In order to predict in advance the coal and gas outburst risks in the No. 3 coal seam in the non-mining area of the Xinjing mine, the strata were divided into seven rock assemblage types based on the lithologic characteristics of strata in the research area, and eight geological profile models were constructed. The finite element methods were used to simulate the ground stress field of the No. 3 seam floor. Based on the log curve, the coal structural type of the No. 3 coal seam was identified, with the thicknesses of the coal body under different types of damage being marked off in each borehole. A damage index of the coal structure (*DV*) was also proposed, and the *DV* indexes for all boreholes were calculated. The coal and gas outburst risks in the research area were comprehensively evaluated and predicted through a superposition analysis of the spatial distribution states of three indexes, namely: ground stress, coal structure damage degree, and coal seam gas content. The results show that the equivalent stress of the No. 3 coal seam floor is usually within the range of 9–26 MPa. The high-stress zone presents a strip distribution along the northeast–southwest (NE–SW) direction. The distribution of ground stress is mainly subject to the folds and buried depth of the coal seam. The distribution range where the damage degree of the coal structure falls under Types II and III is $DV \geq 22$. The gas outburst risk in the mid-southern and northeastern parts of the research area is high, whereas that in the mid-western part is low. The zones with a high and low degrees of gas outburst risks are all mainly present as strips in the NE–SW direction. The gas outburst risk in the northwest and southeast is moderate. The research results can provide guidance for gas control in non-mining areas.

Keywords: ground stress; simulation; gas; gas outburst risks; advanced prediction

1. Introduction

Although the Chinese government has been strengthening the prevention and control of coal mine gas accidents, gas accidents still account for a large proportion of major coal mine accidents [1]. Gas is derived from coal bed methane (CMM). On the one hand, it poses a threat to the safety of coal production, while on the other hand it could be used for clean energy. The utilization of gas can help reduce greenhouse gas emissions [2].

The spatial distribution of gas content is controlled by the geological structure, because regional and mine structures form different sealing conditions which control the distribution of gas content in the coal seam [3]. At the same time, the tectonic deformation and tectonic deformed coals have

an important impact on gas (or coal bed methane) accumulation. In a mining area for example, the development of mylonitized coal (one kind of tectonic deformed coal that exhibits strong deformation) is not conducive to drainage [4]. Of course, the preservation conditions for gas after accumulation are also crucial. For instance, when coal bearing strata in some mining areas were raised and eroded, this type of tectonic evolution background was not conducive to gas preservation [5].

Gas emission during the mining process is affected by various factors. During exploiting, the annular-shaped overlying zone formed around the longwall panel could cause rock stress change, which then accelerates the development of cracks, and affects the gas flow pattern [6]. A test conducted in the field has shown that there is a good correlation between rock burst and high methane gas emission events [7]. The development of minor fault groups in a coal mine and its various combinations significantly affect gas emissions. For example, small, closed faults could create a sealed space so that gas could easily accumulate [8]. In addition, the amount of gas emission is also related to the content of the vitrinite group of coal rock: the amount of coal gas emission with a higher content of the vitrinite group is higher [9].

The mechanism of gas migration has been studied through experimentation, and its behavior has been investigated via numerical simulation. Experimental studies have demonstrated that gas seepage in coal seams is mainly influenced by the effective stress effect, shrinkage effect of the coal matrix, gas slippage effect, and the effect of the superposition of these variables [10]. It has been reported that the highest permeability is in the direction parallel to the bedding surface. Therefore, gas seepage can easily occur along the direction of the bedding surface [11]. An experiment comparing primary structural coal and molded coal showed that different coal structures may react differently during the adsorption–desorption process and with a change of residual strains after desorption [12]. In order to study the gas migration pattern, FLAC 3D and other numerical simulation methods are often employed to study stress distribution in the mining area. The gas–solid constitutive coupling model that takes gas pressure and the adsorption effect into consideration can be derived with COMSOL software, and it can then be used to simulate gas migration in front of the working face, and to study the pattern of gas migration in the coal seam [13].

Coal and gas outburst is a strong gas dynamic phenomenon, and a lot of research has been done in this field. This gas dynamic phenomenon in coal mines is closely related to ground stress and the thickness of the coal seam [14]. In addition to the closure effect of the roof and the floor, the area around the high density-gas zone in the coal seam is often a circular, low-permeability zone that causes an abnormal enrichment of the gas distribution in the coal seam, thus providing the conditions necessary for coal and gas outbursts [15]. Experiments on a briquette body have shown that the smaller the coal particle size, the larger the fractal dimension of the coal pore structure. Therefore, the adsorption capacity for gas is strong, and the strength of the coal and gas outburst is high [16]. In summary, it has been well understood that accidents resulting from coal and gas outbursts in mining areas are mainly affected by the geological structure, the mining depth, the thickness of the coal seam, the lithology of the roof and floor, the physical properties of coal, the gas content, and the mining methods [17,18].

Different field test data must be used to evaluate the coal and gas outburst risks with the aid of an approach based on a mathematical method and artificial intelligence. In the early stage, the critical value of gas outbursts was defined by the amount of drillings and the rate of flow of gas [19]. Some scholars also discussed the relationship between the anomalous electromagnetic radiation of rocks, the EPR spectra of coals and the gas outbursts [20,21]. Another model was dichotomic functions based on a random field to represent relations between the causes and effects of outbursts [22]. In the last 10 years, researchers installed meters and gauges in a pit to regularly measure gas pressure and its change pattern, and then calculated the coal seam permeability in order to control the gas outburst risks [23]. Using Monte Carlo techniques, several scholars collected data during field testing and laboratory tests and then applied a model grid to simulate and analyze the gas outburst risks [24]. Other scholars have tried to obtain the precise content of gas in coal seams by using a rapid field sampling technique aided by instruments and in combination with numerical simulations, in order to

improve the scope and efficiency of gas outburst predictions [25]. The artificial neural network (ANN) can be used to calculate the interconnection weight of indexes, and an index evaluation method (EEM) can be employed to classify the levels of the gas outburst risks [26]. By combining a fuzzy system with a neural network, a method for evaluating the gas outburst risks based on the fuzzy neural network can be established [27,28]. In addition, based on a logic regression model, Li et al. (2015) proposed an approach to evaluating the gas outburst risks method [29].

Currently, mining technology with a protective layer is the primary means by which attempts to prevent coal and gas outbursts are made. The main purpose of this technology is to promote stress release and crack development in the protected layer, which favors gas extraction. This approach is the most effective and economical method for preventing coal and gas outburst risks, and includes a far-distance protection layer, a self-protection layer made of a thin coal bed, and other techniques [30–33].

Based on the literature review, one can see that many in-depth studies have been conducted on the gas accumulation mechanism in coal seams and on gas emission and migration during mining. These works are generally based on experimental and theoretical analyses. At the same time, gas dynamic phenomena during mining, particularly outburst behavior, are commonly evaluated and predicted by using field test data in combination with numerical simulations and intelligent technology. Such evaluations are usually performed within the limited scope of the working face of the mining area. After understanding the relative mechanism, techniques and measurements are utilized for the prevention and management of gas outbursts. At present, little research focuses on the advanced evaluation and prediction of gas outburst risks in non-mining areas. Conducting an advanced prediction of gas outburst risks in non-mining areas of coal mines is important, as such predictions can provide the basis for decision-making on the mining face layout, selection of mining mode, and technology of gas outburst prevention, in order to ensure the safety of mine production.

Many geological factors might affect gas outbursts, with ground stress, strength of the coal body, and gas content being the three main and direct controlling factors. Studies have shown that tectonic evolution plays a leading role in controlling gas occurrence and migration in coal seams. High gas pressure is formed under high tectonic stress in the coal bearing strata. Tectonic deformed coal formed under strong tectonic movement is characterized by low strength of the coal body and strong gas adsorption and desorption. Ground stress can control the structure of the coal body and gas pressure, thus playing a dominant role in gas outburst disasters [34]. In this study, an advanced comprehensive evaluation and prediction of gas outburst risks will be conducted by performing a ground stress field simulation according to the actual conditions of the mining area. This study's method can be used as a reference in the advanced prediction of gas outburst risks in non-mining areas of coal mines.

2. Geological Background

The research area is located in Yangquan, Shanxi, China (Figure 1). The strata in this area are completely exposed and mainly include those from the Middle Ordovician, Upper Carboniferous System–Lower Triassic System, and Quaternary (Table 1). The object of this study, the No. 3 coal seam, is located in the Shanxi group. The No. 3 coal seam is 0.75–4.31 m thick, with an average of 2.33 m. The structure of the coal seam is simple and its distribution in the formation is stable.

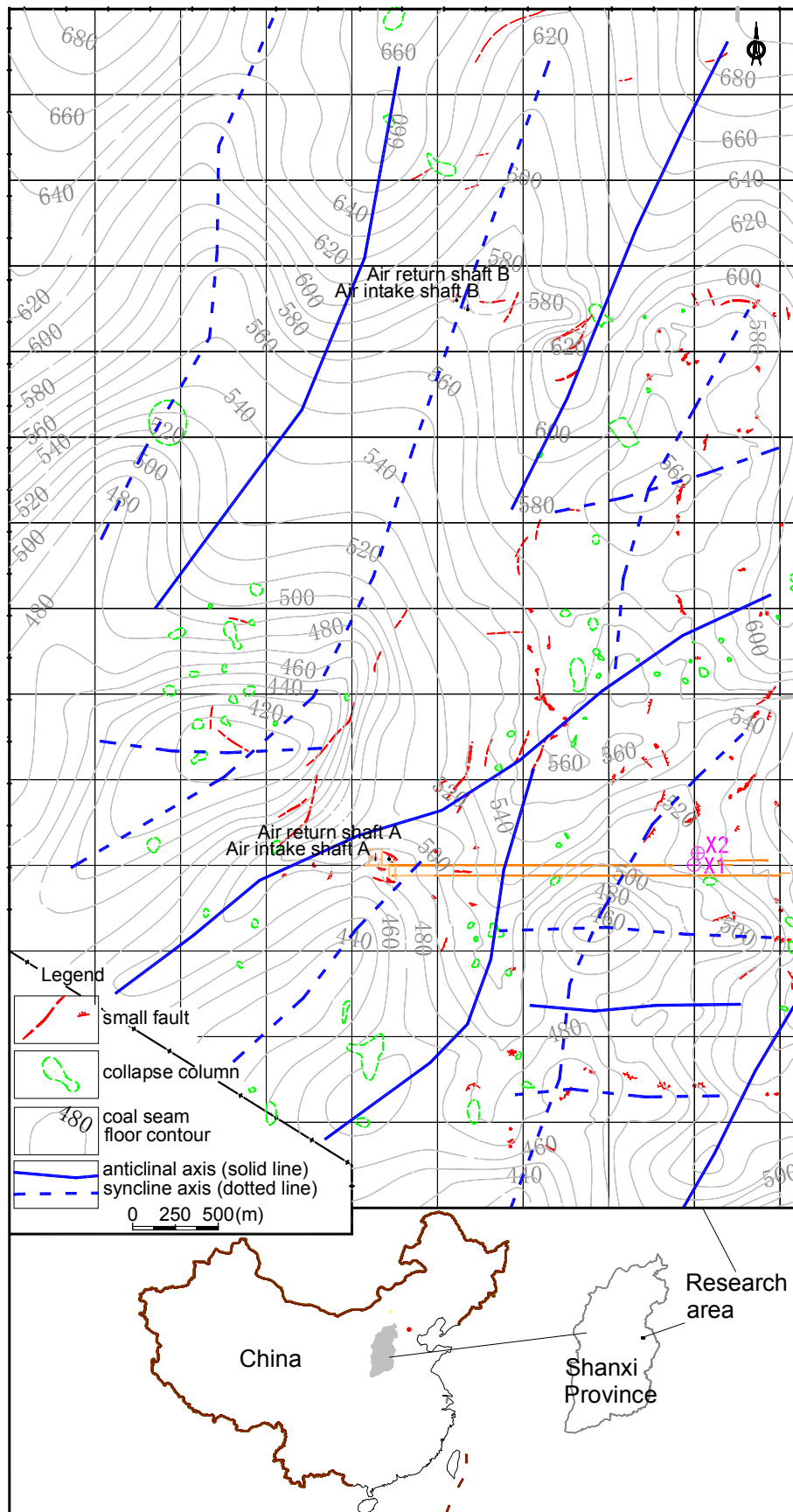


Figure 1. The structural features and geographical position of the research area.

Table 1. Regional stratigraphic table.

Erathem	Stratigraphic Unit			Code	Thickness (m)	Main Lithology
	System	Series	Group			
Cenozoic	Quaternary	Holocene		Q ₄	0–20	Light yellow sandy clay, sand, gravel.
		Middle–Upper Pleistocene		Q ₂₊₃	0–18	Light yellow sandy clay and gravel.
Mesozoic	Triassic	Lower Triassic	Liujagou group	T _{1l}	600	Brick red fine feldspar quartz sandstone, purple red sandy mudstone and lens like interlayer conglomerate.
Paleozoic	Permian	Upper Permian	Sunjiagou group	P _{3s}	80–166	Purple red sandy mudstone and feldspar quartz sandstone.
		Middle Permian	Upper Shihezi group	P _{2s}	396–456	Purple red sandstone, mudstone and sandy mudstone.
			Lower Shihezi group	P _{2x}	97–158	Sandy mudstone, quartzite and aluminum mudstone.
		Lower Permian	Shanxi group	P _{1s}	45–110	Sandstone, mudstone, sandy mudstone, coal seam.
	Carboniferous	Upper Carboniferous	Taiyuan group	C _{2-P1t}	90–130	Sandstone, sandy mudstone, limestone, coal seam.
			Benxi group	C _{2b}	15–55	Sandstone, limestone, coal seam and bauxite.
	Ordovician	Middle Ordovician	Fengfeng group	O _{2f}	130–270	Dolomitic limestone, limestone, marlite, plaster layer.
Upper Majiagou group Lower Majiagou group			O _{2sh} O _{2x}	180–275 125–225	Gray dolomite, plaster layer. Dolomitic limestone and marlite.	

The structural features of the research area are characterized by the irregular monoclinic structure of the northeast (NE) high and southwest (SW) low, with a gentle dipping of 3–11°. The fold structure at the secondary level is developed on the monoclinic structure. Multistage folds superimpose on one another. In the research area, large to medium faults are not developed, but small faults are intensively developed. Statistics on 348 measured faults in the No. 3 coal seam show that there are only three faults with a drop of more than 5 m, which constitute less than 1% of all faults. The coal seam is therefore mainly affected by the fold structure (Figure 1). In the whole mining area, 265 collapse columns were revealed, with an average of 4.1 per square kilometer. The concentrated collapse columns in the mined area are as high as 14 per square kilometer. They are oval and round in a plane form, and in profile they have irregular columnar bodies that are wide below and narrow on top. There is no magmatic activity in the research area.

3. Simulation of Ground Stress Field

3.1. Background of Regional Tectonic Stress Field and Measured Ground Stress in the Mining Area

Based on focal mechanism solution data from North China, Cui et al. (2001) calculated and discussed the temporal and spatial variation characteristics of the direction of a modern tectonic stress field [35]. Their research result shows that the azimuth of the modern tectonic stress field in North China is NE–SW, that the intermediate stress is nearly vertical, and that the angle between the maximum principal stress axis and the horizontal plane is about 10°. It can therefore be confirmed that the azimuth of the modern stress field in the research area is NE–SW, and that the maximum principal stress is near the horizontal level.

The ground stress tests had been carried out in the Xinjing coal mine and its surrounding coal mines. Consequently, abundant test data were accumulated in recent years. Ground stress was measured using a hydraulic fracturing method. The test results included vertical stress, minimum horizontal stress, maximum horizontal stress, and the direction of the maximum horizontal stress. The statistics of the ground stress data demonstrated that the vertical and maximum horizontal stresses gradually increased along with an increase of depth, and that they had a good linear relationship (Figure 2). The fitting relationship between the maximum horizontal stress and the depth is

$$\sigma_H = 0.023 \times S + 3.850 \quad (1)$$

where σ_H is the maximum horizontal stress (MPa), and S is the depth (m).

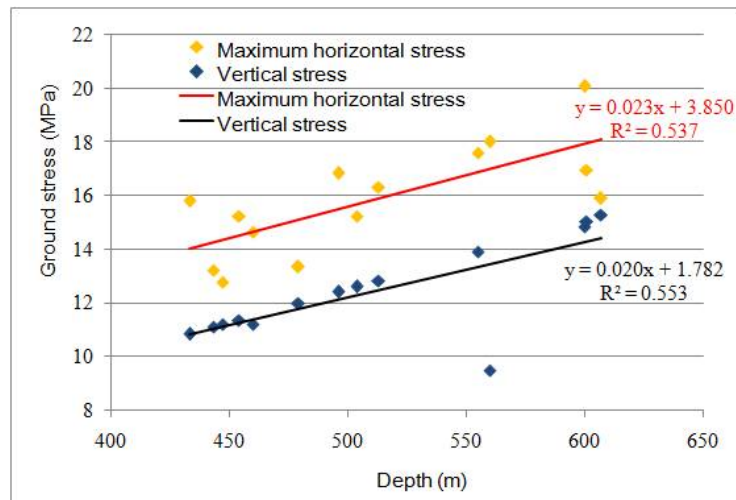


Figure 2. Correlation between ground stress and depth in the research area.

3.2. Determination of Rock Mechanical Parameters in the Research Area

Previous research has demonstrated that a certain relationship exists among different rocks' physical and mechanical indexes. By fitting experimental data on sandstone and those on mudstone, Cao et al. (2010) obtained the relationship between the rock uniaxial compressive strength and the elasticity modulus [36]. Zhang et al. (2011) established a correct empirical formula for the rock internal friction angle (φ) and Poisson's ratio (μ) as follows [37]:

$$\mu = (83 - \varphi) / 163^\circ \quad (2)$$

where μ is Poisson's ratio (dimensionless), and φ is the internal friction angle ($^\circ$).

The above study results are suitable for sedimentary rocks. The strata in the research area are also sedimentary rocks, and there were abundant data from the rock compressive strength test, though there was a lack of results for the elastic modulus and Poisson's ratio; the study results from Cao et al. (2010) and Zhang et al. (2011) were therefore referenced in the below estimation of rock mechanics parameters.

The formation lithology in the research area mainly includes limestone, sandstone, siltstone, shale, sandy mudstone, and coal. According to the physical and mechanical properties, rocks with similar engineering geological properties are combined into a fixed rock assemblage and are divided into six rock groups, namely hard, medium hard, general, medium soft, soft, and extremely soft groups. In addition, a rigid "model cover" was designed to replace other rock assemblages which are located from just above the Shanxi Formation to the surface, excluding a coal bed. Based on the statistical result on the physical and mechanical indexes in the research area in combination with previous study results, the calculation parameters of each rock assemblage were predicted for a numerical simulation, as shown in Table 2.

Table 2. Classification of rock assemblage types and calculation parameters of the simulation in the research area.

Rock Assemblage	Classification	Mechanical Index
The limestone is the main type, and the lithology is relatively simple.	Hard	$E = 40 \times 10^9$, $\mu = 0.28, \rho = 2720$
Medium- and coarse-grained to fine-grained sandstone, sandwiched with thin layers of shale, mudstone and sandy mudstone.	Medium hard	$E = 25 \times 10^9$, $\mu = 0.33, \rho = 2650$
Siltstone is the main type, or a sandstone and shale interbed development.	General	$E = 20 \times 10^9$, $\mu = 0.35, \rho = 2640$
Shale and sandy mudstone are the main ones, sandwiched with fine sandstone—siltstone or thin layer of limestone.	Medium soft	$E = 15 \times 10^9$, $\mu = 0.36, \rho = 2640$
Coal bearing strata, composed of sandy mudstone, shale, marlite or thin layer of limestone, siltstone, and sandwiched with thin coal seam.	Soft	$E = 10 \times 10^9$, $\mu = 0.38, \rho = 2620$
Coal seams and carbonaceous shale roof.	Extremely soft	$E = 5 \times 10^9$, $\mu = 0.40, \rho = 1420$
Model cover (designed according to rigid body)	Highly rigid body	$E = 100 \times 10^9$, $\mu = 0.01, \rho = 2650$

Notes: E is modulus of elasticity (Pa), μ is Poisson's ratio (dimensionless), and ρ is the density (kg/m^3).

3.3. Geological Modeling from Cross-Profile and Finite Element Simulation of Ground Stress

A geological model was established from the cross-profile according to the following principles.

- (1) A number of 2D geometric models were established after examining the geological profile. The azimuth of the geological profile was determined by the maximum horizontal principal stress orientation of the modern stress field in the region. By taking the measured ground stress results in Xinjing Mine into consideration, it was determined that the azimuth of the maximum horizontal stress was about 51° . In consequence, the 2D geometric models were constructed based on eight designed geological profiles. The locations of these geological profiles, I–VIII, are shown in Figure 3.
- (2) The tectonic characteristics of Xinjing Mine were mainly manifested as folds and superpositions of folds. Large to medium faults were not well developed, and faults with less than 5 m of measured drops in the mine comprised over 90% of all faults. Small faults could be ignored after being compared with the size of the simulation profile. Therefore, when the geological geometric model was constructed in the research area, the effect of folds was mainly considered.
- (3) The classification of rock assemblages of various geological profile models was generally consistent. The formation beyond the Shanxi Formation was no longer further divided and was substituted with a rigid cover. Different vertical pressures were provided at the top of the “model cover”, on the basis of formation development, topography, and geomorphology (Figure 4a).

Based on the above principles, 12 rock assemblages were established, while rock formations with similar mechanical properties were merged. Coal seam was treated as a separate layer.

The steps for conducting the finite element simulation on the ground stress are as follows:

- (1) Mesh generation: Considering the irregular thickness and structural type of a stratum, the thin rock formations and the parts with large deformations were encrypted when conducting meshing generation. Taking profile IV as an example, mesh division was carried out in an intelligitized and free manner, with a triangle shape. There were 35,355 nodes and 17,640 units after division. The grid size depended on the thickness of the layer, and the coal seam was regarded as the target layer to be subdivided.
- (2) Boundary constraints: A vertical constraint was adopted for the bottom boundary ($UY = 0$), and a horizontal free constraint was adopted for the lateral boundary (i.e., a roller bearing restraint).

- (3) Model loading: Horizontal pressure stress loading with a triangular distribution was applied to the models according to Equation (1). The gravitational acceleration was set to $g = 10 \text{ m/s}^2$, and the vertical stress was calculated based on the vertical distance from the top of the “model cover” to the ground.
- (4) Operation and results: The stress and strain values on each node were obtained after being calculated. As stress includes the maximum and minimum principal stress and equivalent stress, the equivalent stress (i.e., Von Mises stress) was used to represent the ground stress state (Figure 4b).

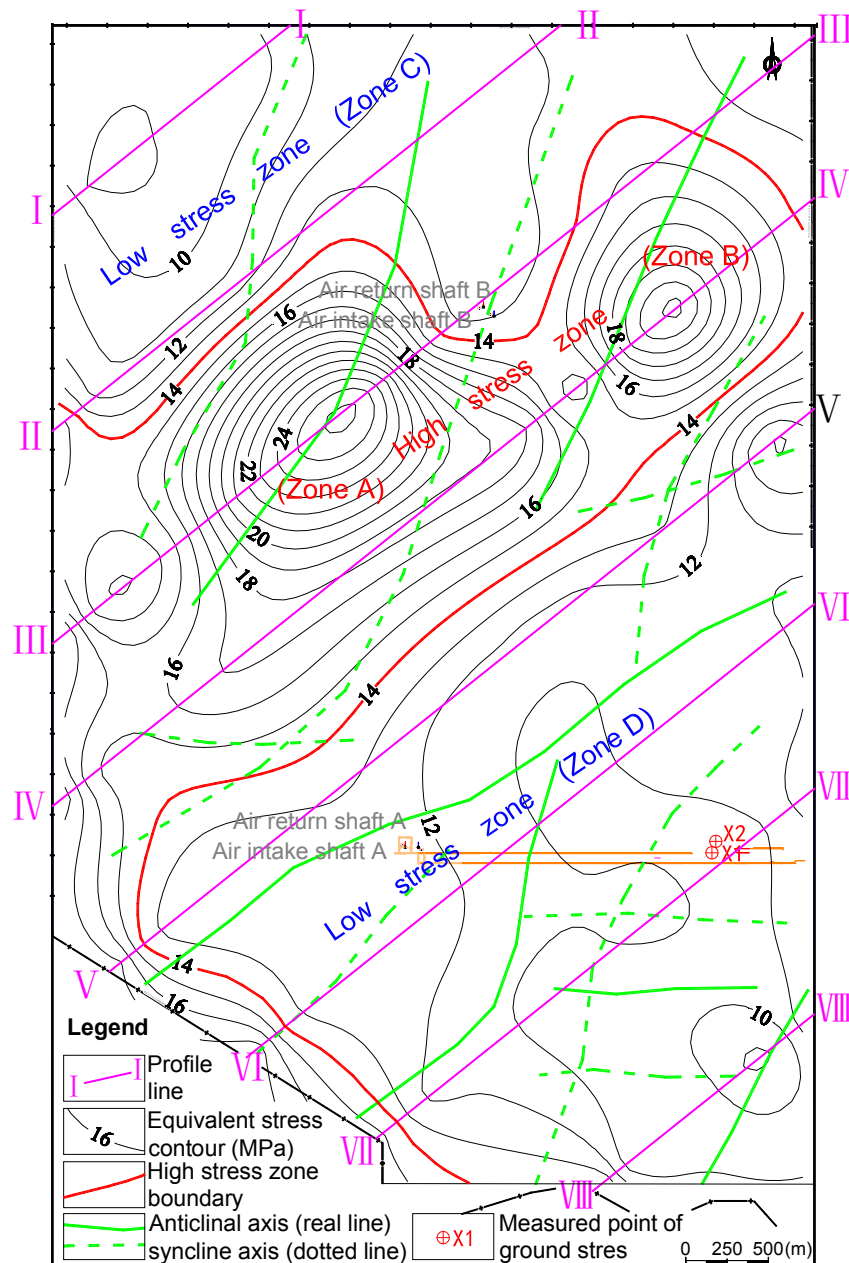


Figure 3. Equivalent stress distribution map of the No. 3 coal seam floor and the positions of the designed profile.

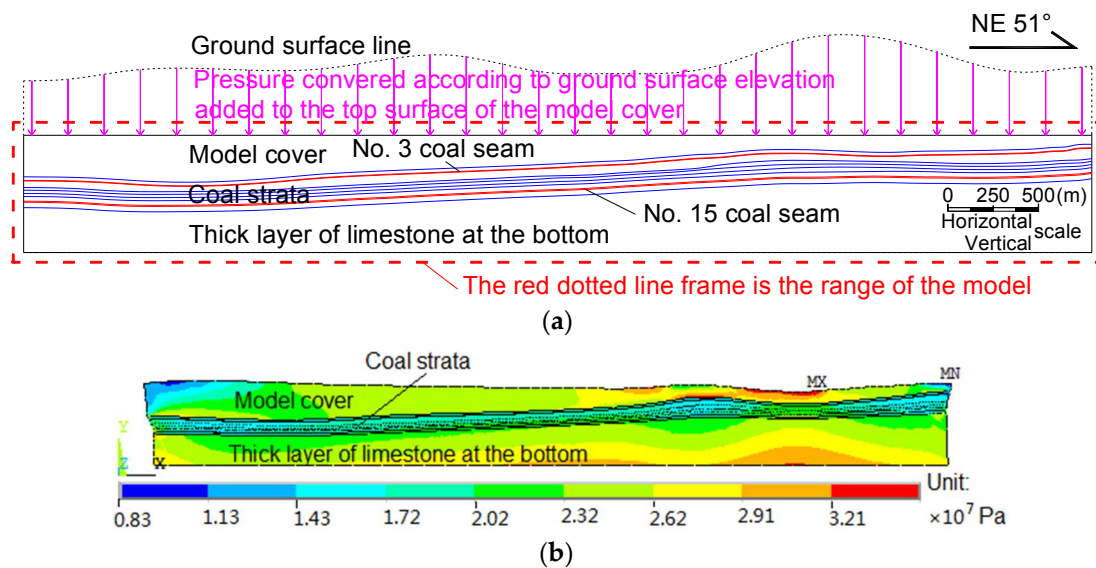


Figure 4. Modeling and simulation results of profile IV–IV. (a) The establishment of a 2D profile geological model; and (b) An equivalent stress cloud map of a profile.

3.4. Distribution of Ground Stress in the Floor of the No. 3 Coal Seam

The stratigraphic profile was divided into a large number of nodes through mesh generation. After being calculated, the nodes were assigned with stress and strain values. A contour map of the stress distribution on the floor of the No. 3 coal seam was obtained after collecting node data in the profile line of the floor of the No. 3 coal seam of model profiles I–VIII (Figure 3), and by kriging interpolation among various profile lines. The results showed that the equivalent stress of the floor of the No. 3 coal seam in the research area was within the range of 9–26 MPa in general, and that the high-equivalent-stress zone showed a strip distribution in the NE–SW direction (Figure 3). There are two ground stress measured points, X1 and X2, that exist in the main roadway in the southeast of the research area. The mean value of the measured maximum horizontal principal stresses is 14.00 MPa. The average sounding is similar to the buried depth of the No. 3 coal seam floor where the simulation was conducted. The simulation result showed that the maximum horizontal principal stress is approximately 12.52 MPa, with a difference of 1.48 MPa from the measured mean value. The difference is about 10.57%, which is within an acceptable range in engineering.

In the contour map of equivalent stresses, the stress gradients on both sides of the 14 MPa stress contour line differ significantly. Taking into account the stress value and stress gradient, the research area was divided into two zones, the “high-stress zone” (Zones A and B) whose stress value is over or equal to 14 MPa, and the “low-stress zone” (Zones C and D) whose stress value is under 14 MPa (Figure 3).

3.5. Discussion of the Ground Stress Field

There is distinct zoning of ground stress in the research area. There is also a direction of the spatial distribution: The high-stress zone (Zones A and B) presents a strip distribution generally in the NE–SW direction, similar to the orientation of the main fold axis in the region. It seems that the zone with a peak value was affected by two groups of anticline axes (Figure 3).

Superimposed folds are highly developed in the research area. In addition to those in the NE–SW direction, there are a few folds near the east–west (EW) direction in the middle-southern to southeastern part (Zone D) (individual in NEE–SWW). Two groups of folds were superimposed with a wide-angle skew or near-vertical intersection. It seems clear that the fold superposition has led to the reduction in ground stress (Figure 3).

The burial depth is also an important factor that affects the ground stress. Based on the above analysis of the measured ground stress, it can be seen that vertical and horizontal principal stresses increase along with the increase of burial depth. The contour line of the coal seam floor in the northwestern part of the research area (Zone C) shows that the burial depth of the coal seam floor in this region is the smallest. Therefore, although this region is also a fold-development zone in the NE–SW direction, without the development of superimposed folds, the ground stress is greatly reduced. It is obviously affected by the shallow buried depth (Figure 3).

In summary, the strength and distribution of ground stress in the research area are mainly affected by the burial depth and geological structure.

4. Advanced Forecast of the Gas Outburst Risks

4.1. Evaluation of the Damage Degree and the Distribution of the Coal Structure

Ground stress, gas content, and strength of the coal structure are the three most important direct factors that control coal and gas outbursts. Therefore, a comprehensive evaluation and prediction of the gas outburst risks in the research area was performed based on the ground stress field, gas content, and development of tectonic deformed coal. Since the spatial distribution characteristics of the ground stress field have already been investigated, the spatial development characteristics of the coal structure must be analyzed further below.

The structural type of the coal body can be divided into three categories according to the logging curve and damage degree: Type I coal, with a good preservation of the primary structure and generally without structural damage, Type II coal, with a damaged primary structure and well-developed fissures, and Type III coal, which has been damaged strongly by tectonic movement and where the primary structure is invisible. Well logging curves have good responses to coal structures. Fu et al. (2003) divided the types of tectonic deformed coal based on different patterns of logging curves [38]. This method had been broadly applied [39]. The logging curves for 112 boreholes in the research area (i.e., the un-mined area of Xinjing Mine) were identified. In the meantime, the structurally deformed coal samples were collected in the mining area for a comparative analysis (Figure 5); the thickness of coal bodies with different structural types in each borehole were determined in this way.

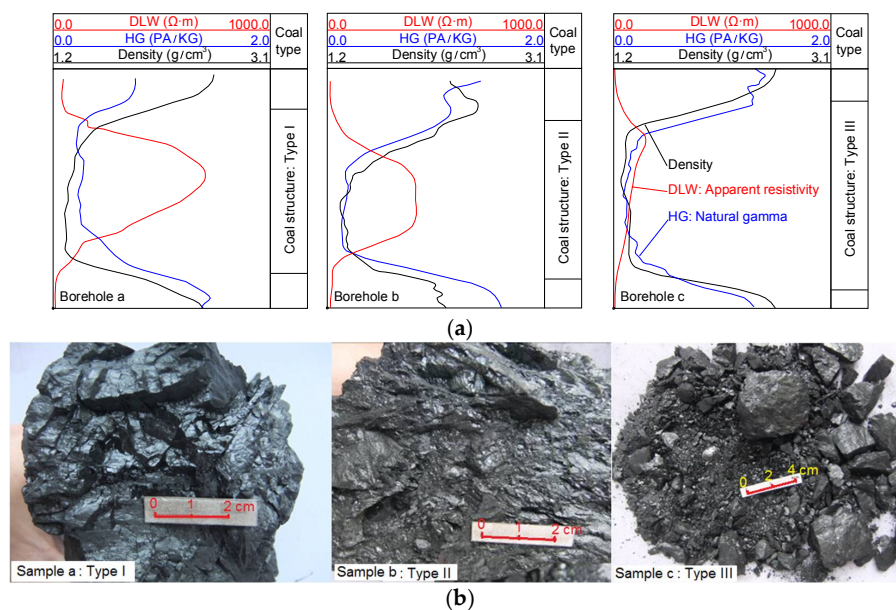


Figure 5. Well logging curves corresponding to different structural types of coals and the apparent characteristics of coals. (a) Well logging curves corresponding to different types of coal structures; (b) and typical samples of different structural types of coal collected in the pit.

In order to perform a comprehensive evaluation of the damage degree of the coal structure, different weights were assigned to Types I, II and III coals by using an expert scoring method: 11, 22, and 67, respectively. The sum of the three values is 100. The damage degree of the coal structure was calculated according to Equation (3).

$$DV = H_I \times 11 + H_{II} \times 22 + H_{III} \times 67 \quad (3)$$

where DV is the damage value of the coal structure, and H_I is the thickness percentage of Type I coal (H_{II} for Type II coal, and H_{III} for Type III coal) in a borehole of the total thickness of Types I, II and III coals in the same borehole.

According to Equation (3), the larger the damage value, the more serious the damage. Only when Types II and III coals are all developed could the damage value of the coal structure exceed 22. Therefore, based on the statistics of 112 boreholes (Figure 6), the development degree of the tectonic deformed coal in the research area was calculated. Using $DV \geq 22$ as the boundary, a distribution map of the tectonic deformed coal was created for Types II and III coals (Figure 6).

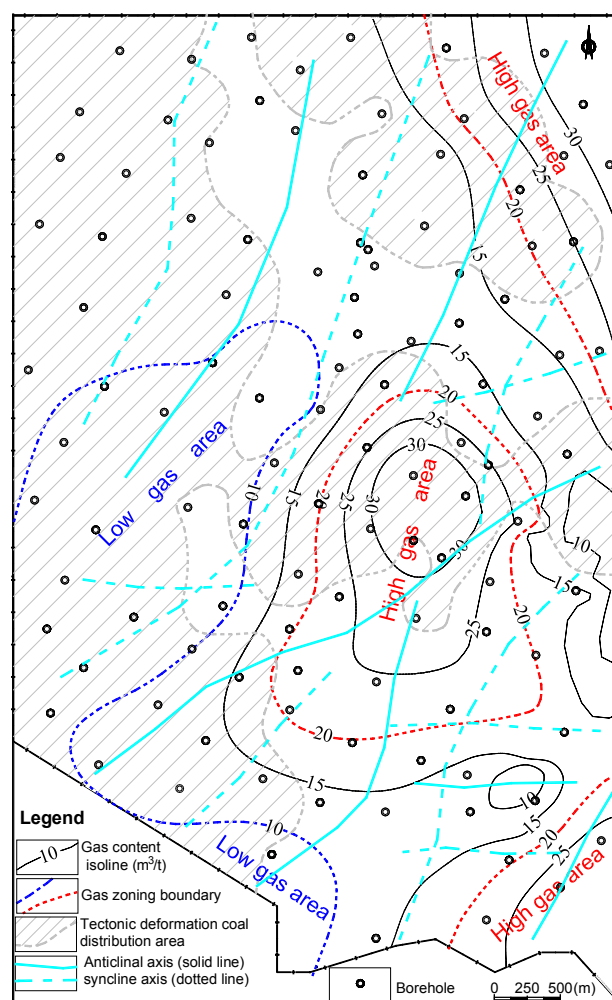


Figure 6. Gas content and distribution of tectonic deformed coal ($DV \geq 22$) of the No. 3 coal seam. Notes: The data of the gas contents in Figure 6 are cited from the report, (Gas occurrence regularity and gas geological prediction in the Xinjing coal mine, Branch project 5: Study of ground stress field). Yangquan Coal Industry (Group) CO., LTD (Yangquan, China), China University of Mining and Technology, March 2018.

4.2. Characteristics of Gas Distribution in the Research Area

According to gas data from the boreholes, the content of gas in the No. 3 coal seam was 10–30 m³/t. The distribution pattern is characterized by high content in the east central–NE corner, slightly higher content in the southeast (SE) corner, and low content in the west central–northwest (NW) and south. The high zone shows a strip distribution in the NE–SW direction. According to the actual value of gas, the research area was divided into three zones: a high-gas zone with a gas content ≥ 20 m³/t, a low-gas zone with a gas content ≤ 10 m³/t, and a medium-gas zone with a gas content between these two values (Figure 6). The gas pressure was 0.4–2.4 MPa, and the absolute gas emission was 6–26 m³/min. The distribution patterns of the gas pressure and absolute gas emission were similar to that of the gas content.

4.3. Evaluation of Gas Outburst Risks with Multiple-Factor Spatial Superimposition and Discussion

The region with coal and gas outburst risks was determined by superimposing the damage value zone of tectonic deformed coal, high-ground-stress zone, and medium-high gas content zone. The results showed that the gas outburst risks in the NE and middle-southern region was high, whereas the risks in the middle-western region was low, with a strip distribution in the NE–SW direction. The gas outburst risks in the NW and SE region is moderate (Figure 7).

The above analysis approach with multiple-factor superposition took ground stress, gas content, and coal structure, i.e., three factors, into consideration. With simulation, statistical analysis, and calculation, the spatial distributions of three factors were obtained. The spatial distributions of these three elements were directly superimposed, in order to perform high and low configuration and partitioning. For safety considerations, conservatism and security were adopted as partitioning principles.

The advantages of this method are twofold. First, the evaluation and prediction of the gas outburst risks can be conducted before mining. There is no need to collect data and perform predictions during the mining process. Therefore, our prediction is advanced in terms of time. Second, such an evaluation and prediction are performed on the entire mining or non-mining areas, rather than on a limited region. Therefore, the prediction scope is wide. Results based on our method could form the basis of decision-making for the layout of a mining area or working face, the selection of a mining mode, and the measures of gas outburst control. Therefore, the method proposed in this paper is significant, as it provides guidance for the safety production in coal mines.

In this study, ground stress, gas content, and coal structure were superimposed and then analyzed directly and evenly. These three elements might have different weights in creating gas outburst risks. If the weight of each factor could be further studied, a partition weighted calculation could be performed. Following this, applying the result in order to predict gas outburst risks would be more reasonable. This could be done in future work.

The research results will guide the design and construction of non-mining areas in the future. It is suggested that when mining in non-mining areas, the areas with low gas outburst risks come first, followed by the moderate risk areas, and then the high risk areas. When mining in areas with low gas outburst risks in this order, the surrounding stress can be released, thereby promoting the desorption and emission of gas in high risk areas. Combined simultaneously with the measures of underground gas drainage, gas outburst risks will be gradually reduced. The specific measures for gas drainage are not discussed in this paper. In addition, if the gas drainage from the ground is considered, the research results in this paper can also provide references for the layout of boreholes.

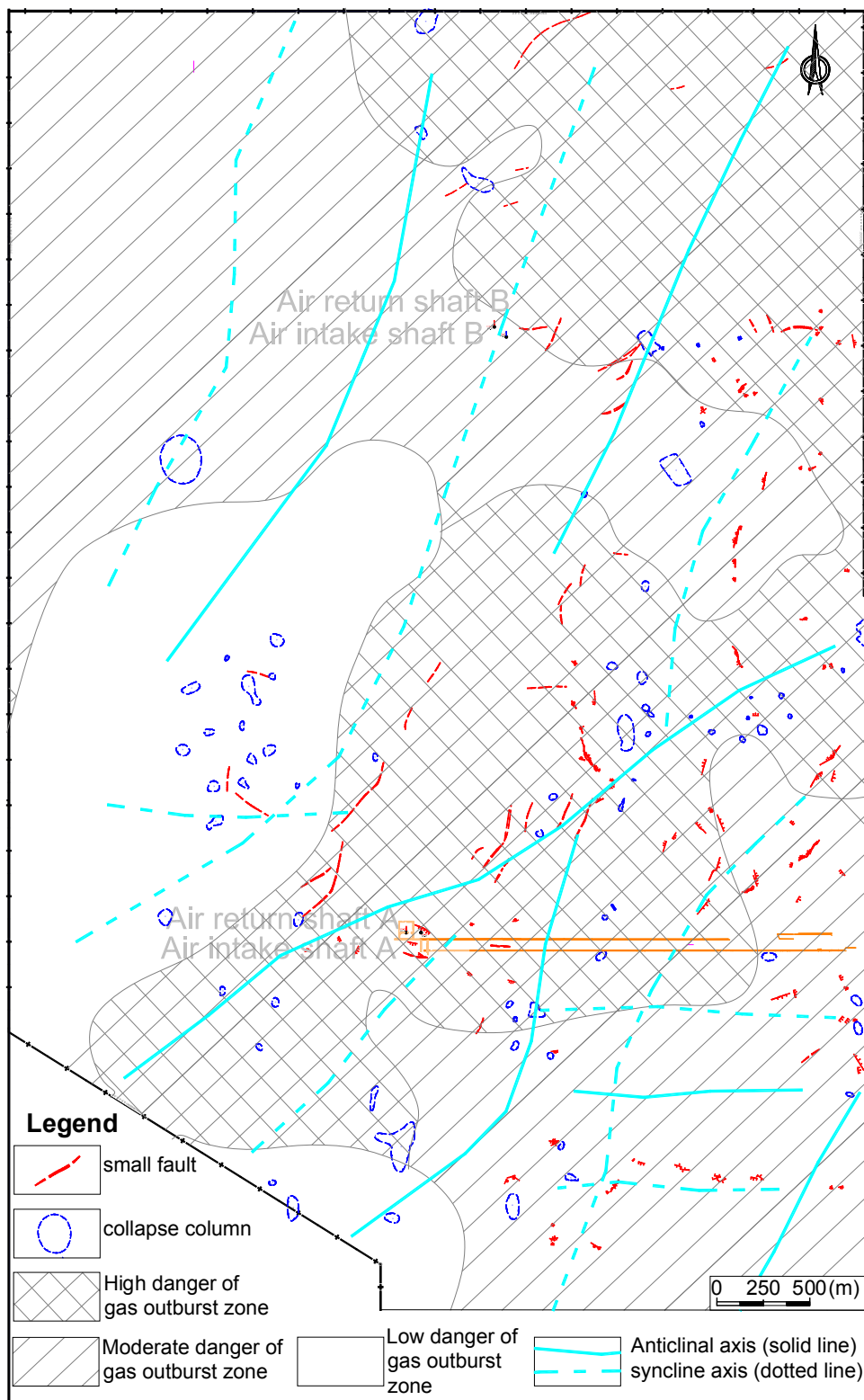


Figure 7. The zoning map of gas outburst risks of the No. 3 coal seam.

5. Conclusions

- (1) The distribution of ground stress in the rock formation of profiles was obtained by performing a numerical simulation of multiple geological profile models. The ground stress value of different profiles on the coal seam floor was extracted and interpolated in space. Following this, the ground

stress distribution on the curved surface of the coal seam floor could be obtained. The results of the simulation showed that the equivalent stress of the No. 3 coal seam floor is generally in the range of 9–26 MPa. The high-stress zone has a strip distribution in the NE–SW direction. The ground stress distribution in the research area is mainly affected by the fold and burial depth of the coal seam.

- (2) According to the tectonic deformation of coal and the damage degree, the coal structure of the No. 3 coal seam was divided into three types, namely: Types I, II and III. The structure types of the coal seam exposed by boreholes were identified according to the logging curve, and have been divided in terms of thickness. A damage index (DV) and calculation method of the coal structure were proposed. Based on the results, $DV \geq 22$ was identified as the boundary to outline the distribution scopes of Types II and III coals.
- (3) Ground stress, damage degree of coal, and gas content are the three major factors affecting gas outbursts. According to the analysis of the three factors superimposed in space, the gas outburst risks of the research area was predicted. The research results show that the gas outburst risks in the mid-southern and northeastern regions were high, and that those in the mid-western regions were low, all with a strip distribution in the NE–SW direction. The gas outburst risks in the northwestern and southeastern regions were moderate.
- (4) It is suggested that when mining in non-mining areas, the areas with low gas outburst risks come first, followed by moderate risk areas, and then finally high risk areas. Through mining in low outburst risk areas, the stress in high risk areas will be released, and gas emission will be promoted, thus reducing the risks of gas outbursts. When extracting gas from the ground, the layout of boreholes can also be designed according to these research results.

Author Contributions: Drafting of manuscript and numerical simulation: J.W.; coal structure analysis: M.L.; interpretation of numerical simulations: S.X.; drawing works: Z.Q.; and planning and supervision of the research: B.J.

Acknowledgments: The authors are grateful for the support of the National Natural Science Foundation of China (41472134 and 41430317) and Natural Science Foundation of Jiangsu basic research program (BK20140183).

Conflicts of Interest: The authors declare no conflict of interest.

References

1. Yin, W.T.; Fu, G.; Yang, C.; Jiang, Z.G.; Zhu, K.; Gao, Y. Fatal gas explosion accidents on Chinese coal mines and the characteristics of unsafe behaviors: 2000–2014. *Saf. Sci.* **2017**, *92*, 173–179. [[CrossRef](#)]
2. Karacan, C.O.; Ruiz, F.A.; Cote, M.; Phipps, S. Coal mine methane: A review of capture and utilization practices with benefits to mining safety and to greenhouse gas reduction. *Int. J. Coal Geol.* **2011**, *86*, 121–156. [[CrossRef](#)]
3. Jang, B.; Qu, Z.-H.; Wang, J.-L.; Li, M.; Dou, X.-Z. Research on coupling mechanism of mine structure and gas occurrence. In Proceedings of the International Conference on Mining Science & Technology (Icmst2009), Xuzhou, China, 18–20 October 2009; pp. 1029–1036.
4. Jiang, B.; Qu, Z.; Wang, G.G.X.; Li, M. Effects of structural deformation on formation of coalbed methane reservoirs in Huaibei coalfield, China. *Int. J. Coal Geol.* **2010**, *82*, 175–183. [[CrossRef](#)]
5. Zhao, Z.; Yan, J.; Liu, X. Research on gas occurrence regularity in Fengcheng Mining Area of Jiangxi Province. *Energy Explor. Exploit.* **2014**, *32*, 591–599. [[CrossRef](#)]
6. Guo, H.; Yuan, L.; Shen, B.; Qu, Q.; Xue, J. Mining-induced strata stress changes, fractures and gas flow dynamics in multi-seam longwall mining. *Int. J. Rock Mech. Min. Sci.* **2012**, *54*, 129–139. [[CrossRef](#)]
7. Li, T.; Cai, M.F.; Cai, M. Earthquake-induced unusual gas emission in coalmines—A km-scale in-situ experimental investigation at Laohutai mine. *Int. J. Coal Geol.* **2007**, *71*, 209–224. [[CrossRef](#)]
8. Ma, S.; Li, Q.; Han, Z.; Zhang, P.; Kang, F. The characteristics of abnormal gas emission in tunneling through the small fault groups of Yizhong coal mine. *Geosyst. Eng.* **2016**, *19*, 232–237. [[CrossRef](#)]
9. Taheri, A.; Sereshki, F.; Ardejani, F.D.; Mirzaghobanali, A. Simulation of macerals effects on methane emission during gas drainage in coal mines. *Fuel* **2017**, *210*, 659–665. [[CrossRef](#)]

10. Wang, J.L.; Qin, Y.; Fu, X.H. Dynamic changes laws of the coal reservoirs permeability under the superimposition of multi influential factors. *J. China Coal Soc.* **2012**, *37*, 1348–1353.
11. Pan, R.; Cheng, Y.; Yuan, L.; Yu, M.; Dong, J. Effect of bedding structural diversity of coal on permeability evolution and gas disasters control with coal mining. *Nat. Hazards* **2014**, *73*, 531–546. [[CrossRef](#)]
12. Zhang, Z.G.; Cao, S.G.; Guo, P.; Liu, Y.B. Comparison of the deformation characteristics of coal in gas adsorption-desorption process for raw and briquette coals. *J. China Univ. Min. Technol.* **2014**, *43*, 388–394.
13. Cao, S.G.; Luo, F.; Liu, Y.B.; Li, Y.; Guo, P.; Li, G.D. Gas migration of coal in front of a mining face considering crack evolution. *Environ. Earth Sci.* **2016**, *75*, 1282. [[CrossRef](#)]
14. Fernandez-Diaz, J.J.; Gonzalez-Nicieza, C.; Alvarez-Fernandez, M.I.; Lopez-Gayarre, F. Analysis of gas-dynamic phenomenon in underground coal mines in the central basin of Asturias (Spain). *Eng. Fail. Anal.* **2013**, *34*, 464–477. [[CrossRef](#)]
15. An, F.H.; Cheng, Y.P. An explanation of large-scale coal and gas outbursts in underground coal mines: The effect of low-permeability zones on abnormally abundant gas. *Nat. Hazards Earth Syst. Sci.* **2014**, *14*, 2125–2132. [[CrossRef](#)]
16. Xu, J.; Liu, D.; Peng, S.J.; Wu, X.; Lu, Q. Experimental research on influence of particle diameter on coal and gas outburst. *Chin. J. Rock Mech. Eng.* **2010**, *29*, 1231–1237.
17. Lama, R.D.; Bodziony, J. Management of outburst in underground coal mines. *Int. J. Coal Geol.* **1998**, *35*, 83–155. [[CrossRef](#)]
18. Zhai, C.; Xiang, X.W.; Xu, J.Z.; Wu, S.L. The characteristics and main influencing factors affecting coal and gas outbursts in Chinese Pingdingshan mining region. *Nat. Hazards* **2016**, *82*, 507–530. [[CrossRef](#)]
19. Ryncarz, T.; Majcherczyk, T. Index of Coal and Gas Outbursts Hazards Taking into Account the Geomechanic and Gaseous Factors. *Prz. Gorniczy* **1982**, *38*, 1–8.
20. Frid, V. Electromagnetic radiation method for rock and gas outburst forecast. *J. Appl. Geophys.* **1997**, *38*, 97–104. [[CrossRef](#)]
21. Lyubchenko, L.S.; Veretil'ny, A.Y.A.; Printsev, E.V.; Kozhushner, M.A. On the possibility of predicting the degree of coal outburst danger by EPR with a high static gas pressure. *Sol. Fuel Chem.* **1996**, *30*, 28–34.
22. Cyrul, T. Prediction of rock and gas outburst occurrence. *Eng. Geol.* **1993**, *33*, 241–250. [[CrossRef](#)]
23. Aguado, M.B.D.; Nicieza, C.G. Control and prevention of gas outbursts in coal mines, Riosa-Olloniego coalfield, Spain. *Int. J. Coal Geol.* **2007**, *69*, 253–266. [[CrossRef](#)]
24. Wold, M.B.; Connell, L.D.; Choi, S.K. The role of spatial variability in coal seam parameters on gas outburst behaviour during coal mining. *Int. J. Coal Geol.* **2008**, *75*, 1–14. [[CrossRef](#)]
25. Yuan, L.; Xue, S.; Xie, J. Study and application of gas content to prediction of coal and gas outburst. *Coal Sci. Technol.* **2011**, *29*, 47–51.
26. He, X.; Chen, W.; Nie, B.; Zhang, M. Classification technique for danger classes of coal and gas outburst in deep coal mines. *Saf. Sci.* **2010**, *48*, 173–178. [[CrossRef](#)]
27. Suarez Fernandez, M.; Lopez, G.; Hilario, R.; Alvarez, A. Fuzzy system for coal and gas outburst risk assessment. In Proceedings of the International Symposium APCOM, London, UK, 19–23 April 1998; pp. 145–148.
28. Liu, H.; Wang, F. Evaluation Strategy of Mine Gas Outburst Risk Level Based on Fuzzy Neural Network. In Proceedings of the 2015 Chinese Intelligent Systems Conference; Jia, Y., Du, J., Li, H., Zhang, W., Eds.; Springer: Berlin, Germany, 2016; pp. 435–441.
29. Li, Z.; Wang, E.; Ou, J.; Liu, Z. Hazard evaluation of coal and gas outbursts in a coal-mine roadway based on logistic regression model. *Int. J. Rock Mech. Min. Sci.* **2015**, *80*, 185–195. [[CrossRef](#)]
30. Li, W.; Cheng, Y.-P.; Guo, P.-K.; An, F.-H.; Chen, M.-Y. The evolution of permeability and gas composition during remote protective longwall mining and stress-relief gas drainage: A case study of the underground Haishiwan Coal Mine. *Geosci. J.* **2014**, *18*, 427–437. [[CrossRef](#)]
31. Liu, H.; Cheng, Y. The elimination of coal and gas outburst disasters by long distance lower protective seam mining combined with stress-relief gas extraction in the Huaibei coal mine area. *J. Nat. Gas Sci. Eng.* **2015**, *27*, 346–353. [[CrossRef](#)]
32. Jin, K.; Cheng, Y.P.; Wang, W.; Liu, H.B.; Liu, Z.D.; Zhang, H. Evaluation of the remote lower protective seam mining for coal mine gas control: A typical case study from the Zhuxianzhuang Coal Mine, Huaibei Coalfield, China. *J. Nat. Gas Sci. Eng.* **2016**, *33*, 44–55. [[CrossRef](#)]

33. Li, D. Mining thin sub-layer as self-protective coal seam to reduce the danger of coal and gas outburst. *Nat. Hazards* **2014**, *71*, 41–52. [[CrossRef](#)]
34. Cheng, Y.-P.; Zhang, X.-L.; Wang, L. Controlling effect of ground stress on gas pressure and outburst disaster. *J. Min. Saf. Eng.* **2013**, *30*, 408–414.
35. Cui, X.F.; Xie, F.R. The Space-time Variations of Present Tectonic Stress Field in North China before and after 1976 Tangshan Earthquake. *Earthq. Res. China* **2001**, *17*, 280–288.
36. Cao, H.; Yang, X.-C.; Xie, L.-K.; Guo, L.-J. Study on rock mechanical properties and the correlation of the mechanical parameters of a mine. *China Min. Mag.* **2010**, *19*, 84–87.
37. Zhang, N.; Sheng, Z.; Li, X.; Li, S.; He, J. Study of relationship between poisson's ratio and angle of internal friction for rocks. *Chin. J. Rock Mech. Eng.* **2011**, *30*, 2599–2609.
38. Fu, X.-H.; Jiang, B.; Qin, Y.; Ye, S.-Z.; Zhang, Y.-G.; Zeng, Q.-H. Classification of Coalbody Structure and Prediction of Coal Reservoir Permeability with Log Curves. *Well Logging Technol.* **2003**, *27*, 140–143.
39. Xu, Q.L.; Huang, W.-H.; Yang, Y.-H.; Liu, B. The study of identifying deformed coal by logging curve on coalbed methane development. *Appl. Mech. Mater.* **2014**, *675–677*, 1347–1350. [[CrossRef](#)]



© 2018 by the authors. Licensee MDPI, Basel, Switzerland. This article is an open access article distributed under the terms and conditions of the Creative Commons Attribution (CC BY) license (<http://creativecommons.org/licenses/by/4.0/>).